PNAS
www.pnas.org

Supplementary Information for

Electrometry by optical charge conversion of deep defects in 4H-SiC

G. Wolfowicz, S. J. Whiteley and D. D. Awschalom

D. D. Awschalom.
E-mail: awsch@uchicago.edu

This PDF file includes:

Figs. S1 to S5

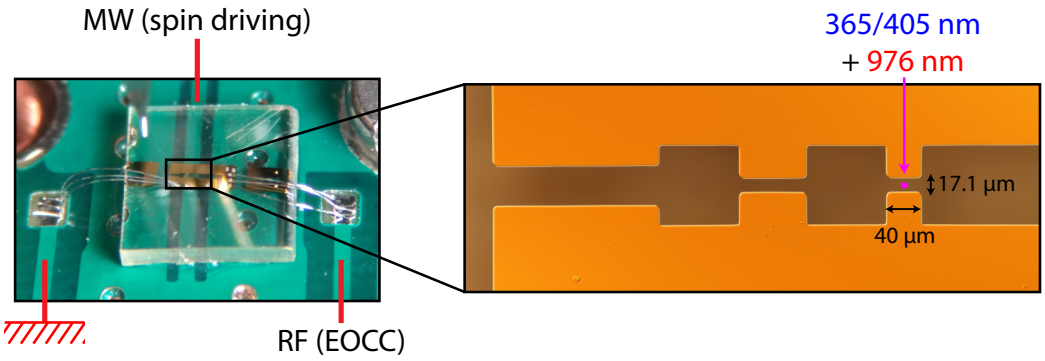

Fig. S1. Microscope images of the capacitor device for EOCC characterization. 4H-SiC sample with electrodes (capacitor) mounted on a printed circuit board with radio-frequency (RF) input for the EOCC electric field signal. A shorted microwave coplanar stripline is directly beneath the sample to allow spin measurements for testing purposes (e.g. confirming the PL signal comes only from VV). The 976 nm laser, 365 nm light emitting diode and 405 nm laser are all focused between two metal gates separated by 17.1 μm.

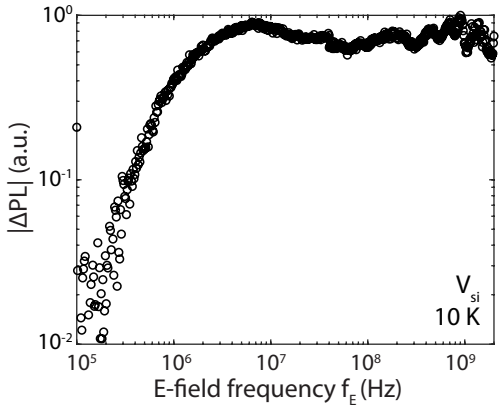

Fig. S2. Frequency dependence of EOCC using V_{Si} in 4H-SiC. Measurement was realized using continuous-wave 785 nm and 365 nm illumination. No significant difference was observed between V_{Si} and VV, showing that the electrometry mechanism is likely identical.

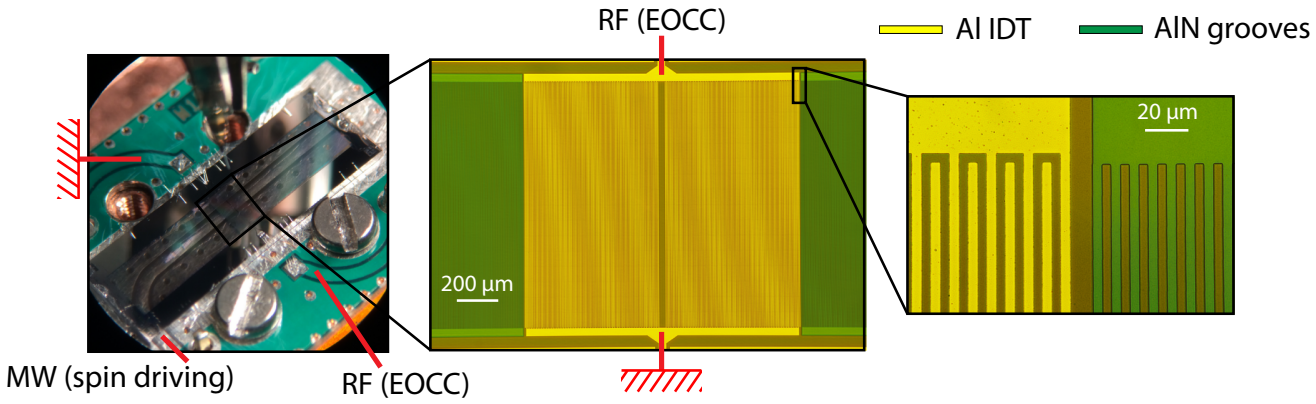

Fig. S3. Microscope images of the surface acoustic wave (SAW) resonator. SAW resonator sample mounted on a printed circuit board with radio-frequency (RF) input for the EOCC electric field signal. A shorted microwave coplanar stripline is directly beneath the sample to allow spin measurements for testing purposes (e.g. confirming the PL signal comes only from VV). The sample has an AlN layer on top of the 4H-SiC substrate with Al interdigitated transducers (yellow) deposited on top of the AlN for driving the SAW. Grooves (green) were etched in the AlN to create the reflectors of the cavity.

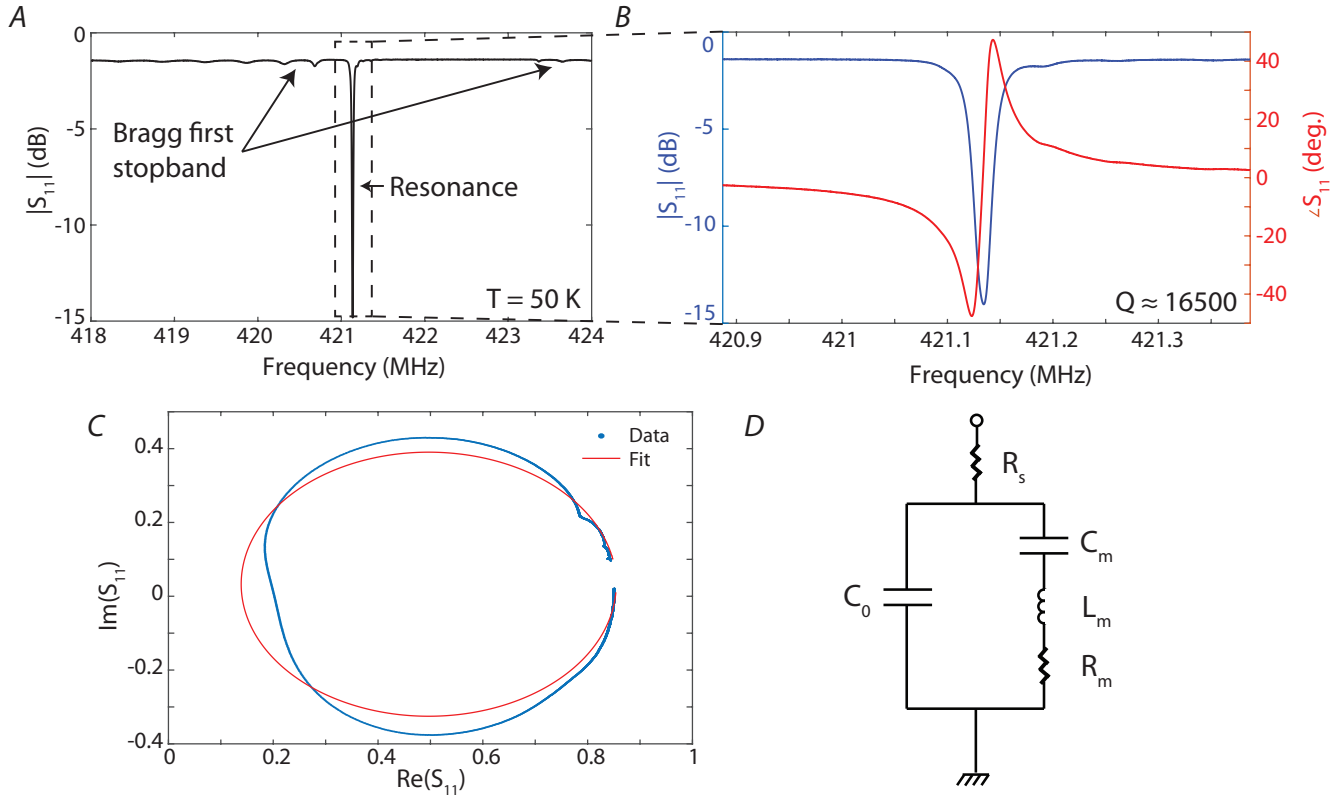

Fig. S4. Electrical characterization of the SAW resonator. *(A)* $|S_{11}|$ reflectivity measurement (magnitude) at 50 K using a vector network analyzer (VNA). *(B)* Zoom in on the resonance in *A*, with both the phase and magnitude of the $|S_{11}|$ response. The quality factor Q is about 16500. *(C)* Polar plot of the $|S_{11}|$ reflectivity measurement. *(D)* Equivalent circuit of the SAW using a modified Butterworth-Van Dyke (MBVD) filter. The geometric capacitance $C_0 \approx N_\mathrm{p} W \epsilon_\infty = 18.70$ pF, with N_p the number of electrode finger pairs, W the aperture or transverse length of capacitor overlap and $\epsilon_\infty \approx 11\epsilon_0$ the dielectric constant (adjusted for IDT calculations) of 4H-SiC. The fitted parameters in the model from the data at 50 K are: the resonator capacitance $C_\mathrm{m} = 1.69$ fF, the resonator inductance $L_\mathrm{m} = 84.6$ μH, the resonator resistance $R_\mathrm{m} = 10.3\ \Omega$ and the external stray resistance $R_\mathrm{s} = 4.45\ \Omega$. R_s is likely from losses in the cables, the printed circuit board and the coplanar waveguide to the sample.

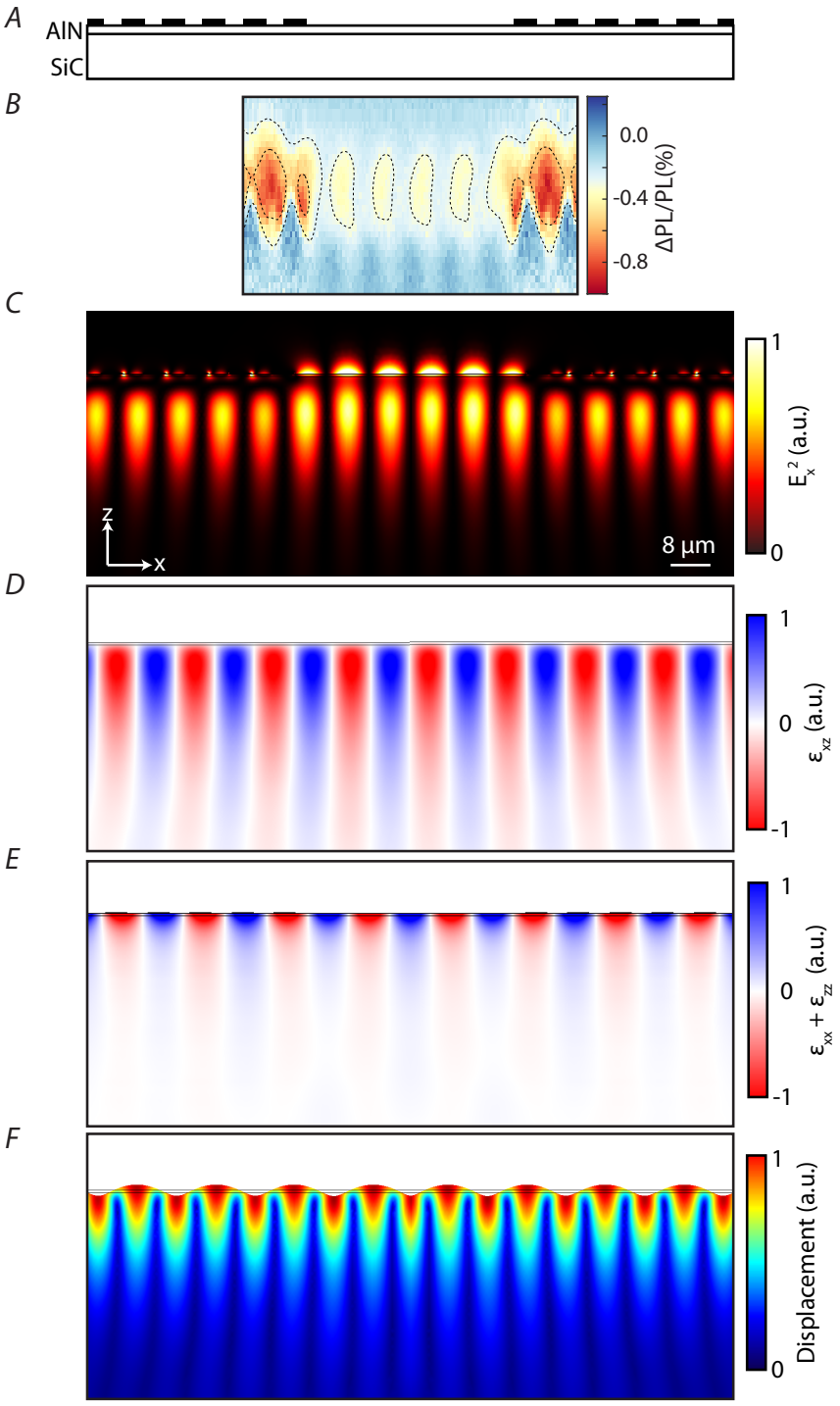

Fig. S5. Numerical simulations (COMSOL) of the electro-mechanical mode of the SAW resonator. *(A)* Schematic of layers in de SAW device. *(B)* EOCC contrast (see Figure 4. of the main text). COMSOL simulations are given from *C* to *F*: *(C)* x component of the electric field (square). *(D)* ϵ_{xz} shear. *(E)* Volumetric strain. *(F)* Displacement. All simulations were obtained when the voltage across the IDT is close to zero. In this case, the dominant contribution is the build-up strain, shear and piezoelectric field of the SAW resonator. This is in contrast with the experimental result in *B* where the amplitude is larger beneath the metal. In addition, the simulation does not take into account all interdigitated fingers and reflectors.